Proceedings of the Twenty-fifth (2015) International Ocean and Polar Engineering Conference **www.isope.org**
Kona, Big Island, Hawaii, USA, June 21-26, 2015

ISBN 978-1-880653-89-0; ISSN 1098-6189

Effects of a higher Reynolds number and introduced perforation on flows past the conic cylinder

Liming Lin, Xingfu Zhong, Yingxiang Wu
Key Laboratory for Mechanics in Fluid Solid Coupling Systems, Institute of Mechanics, Chinese Academy of Sciences.
Beijing, China

ABSTRACT

Through numerical simulations, effects of a higher Reynolds number (10^5) and the introduction of perforation at a lower Reynolds number (10^2) on flows past a circular cylinder with the conic disturbance are investigated. Particularly, circular holes are located on and uniformly distributed around the peak of the conic shroud. Results have been shown that the higher Reynolds number of 10^5 has little effect on qualitative variations of the drag and lift coefficients and the frequency of vortex shedding in most cases, which are almost similar to those at lower Reynolds numbers, as well as the introduced perforation. Nevertheless, there are still several exceptional cases with different hydrodynamic parameters resulted from the introduction of perforation. And different disturbance regimes and vortex patterns in the near wake for these cases are identified and presented in detail.

KEY WORDS: Numerical simulations; circular cylinder; conic disturbance; perforation; vortex-induced vibration.

INTRODUCTION

A straight and long cylinder is a common structure as a bluff body in many engineering applications, such as mooring cables, flexible risers and pipelines in the platform of oil production and marine engineering, suspension bridges. The incoming flow past such cylinder results in the unsteady wake and alternatively shedding vortex behind the body. Consequently, the body would be vibrated due to the unsteady fluid forces acted on the body, called vortex-induced vibrations (VIV). In particular, as the frequency of vortex shedding approaches the natural frequency of structure, the lock-in of frequency is occurred with the resonance. Meantime, the structural oscillating amplitude, as well as the fluid force, would be grown rapidly. This further leads to high possibility of structural fatigue damage and dangers the safety of people, even production activity. Hence, a great number of researches have been published in understanding the dynamics of VIV in a half century. Comprehensive reviews can be referenced in Sarpkaya (1979), Sarpkaya and Isaacson (1981), Sarpkaya (2004), Williamson and Govardhan (2004; 2008), and Gabbai and Benaroya (2005).

With the aim of weakening unfavorable effects of VIV and improving structural validity, many methods have been proposed over recent several decades. The physical mechanism is mainly attributed to control the wake dynamics through weakening the vortex shedding, even totally suppressed, as well as amplitudes of fluid forces, or mismatching the frequency of vortex shedding far away from the natural frequency of structure. For example, the surface control bump spirally distributed around the cylinder, proposed by Owen *et al*. (2001), could reduce the drag about 47%. At a certain wave steepness, defined by the ratio of the wave height to the wavelength of such disturbance, any sign of vortex shedding was no longer detected. However, such device was mainly effective in the higher mass-damping parameter. Two small rotating cylinders arranged in the boundary layer of the cylinder, proposed by Korkischko and Meneghini (2012), could delay the separation of the boundary layer away from the surface of cylinder. The drag reduction was also reached up to almost 60%. As a kind of the passive control method, the triple-starting helical grooves (Huang, 2011), multiple control rods (Wu, et al., 2012) and ventilated trouser (King, et al., 2013) were recently proposed and investigated. So far, the streamline fairing (Lee and Allen, 2005) still exhibits a very good aerodynamic performance due to the streamlined outer shape and the resultant of the delay of the flow separation. Similarly, splitter plates can effectively delay the interaction between upper and lower shear layers too and therefore the formation of vortex shedding (Assi, et al., 2009). Due to the uncertainty of ocean flow direction, the rotatable device is commonly applied for the streamline fairing and splitter plates. This then would introduce a new dynamical instability. Helical strake (Trim, et al., 2005; Korkischko and Meneghini, 2010), as a way of disturbance on spanwise uniformity of vortex shedding, is the most widely used presently. More information about them can be found out in review works by Sarpkaya and Isaacson (1981), Kumar et al. (2008), and Wu and Sun (2009).

On the other hand, there is another VIV suppressing method proposed by introducing three-dimensional geometric disturbance, such as a wavy front surface (Bearman and Owen, 1998) and totally wavy cylinders (Owen, et al., 1999; Darekar and Sherwin, 2001; Lin, et al., 2010). Such disturbance is introduced in a streamwise-spanwise plane and thus sensitive to different flow directions. So, A new idea of disturbance introduced in a radial-spanwise plane, called radial disturbance, was proposed by Lin, et al. (2011; 2012), based on the Bernoulli equation and the effect of geometric disturbance on the flow

past the bluff body. For verification of such idea, experiments for VIV of pendulum with two radial disturbances, harmonic and conic-like, in water channel were carried out. Results have shown that the oscillating amplitude is reduced greatly at the start of lock-in, but increased at a higher reduced velocity. This indicates that the frequency of vortex shedding is reduced by the radial disturbance, also confirmed by later numerical simulations (Lin, et al., 2013; 2014b). For the intrinsic difference between pendulum and riser, the flow around the fixed cylinder with circular section and two types of radial disturbances, harmonic and conic, was numerically simulated to investigate the physical mechanism and effects of such radial disturbances. At Reynolds number of 100, the variation of hydrodynamic parameters, such as lift and drag coefficients, vortex patterns in the near wake summarized as shown in Fig. 1 with the correction, and other flow characteristics for two disturbances are qualitatively similar with the variation of wave steepness. At the Reynolds numbers of 10^2, 10^3 and 10^4 for flows past the cylinder with the conic disturbance, as the wave steepness increases, the drag is generally increased, while the lift in most cases is reduced quickly at first and then increased slowly. The Strouhal number is generally decreased with the increasing wave steepness. However it is still not clear whether these features above would be hold at the higher Reynolds number, such as 10^5.

Furthermore, an improvement in the conic disturbance is applied. The numerical results (Lin, et al., 2014a) have already shown that the time-averaged pressure at the peak of conic disturbance is obviously greater than that at the valley and the increase of drag is mainly attributed to the great increase of projected area because of the introduction of the conic disturbance. And the perforated shroud with uniform circular section has been already proposed as a kind of method in suppressing VIV over thirty years (recorded in Sarpkaya and Isaacson, 1981). Thus, such improvement, that is the perforation on the conic shroud, is proposed here and arranged uniformly at the peak of shroud.

In the present paper as one of a series of works, one of two purposes is to know qualitative variations of hydrodynamic parameters for the conic disturbance without the perforation at the Reynolds number of 10^5 and compare with those at lower Reynolds numbers. Another is to investigate effects of the perforated conic shroud on the hydrodynamic parameters and vortex patterns in the near wake through numerical simulations at a low Reynolds number of 100 with a series of wavelength and wave steepness. Firstly, the physical model with numerical methods is described briefly. Then results for the conic disturbance without the perforation at a Reynolds number of 10^5 and with the perforation at a Reynolds number of 10^2 are presented and analyzed, respectively. At last conclusions are drawn in brief.

PHYSICAL MODEL

Governing Equations

As shown in Fig. 2, the incompressible flows with constant density ρ and kinematic viscosity v past circular-section cylinders with the conic disturbance, called the conic cylinder, and the perforated conic shroud with circular holes along the span are considered. The peak and valley are defined as spanwise positions with maximal and minimal diameters, respectively. The wavy shape can be mathematically described by the wavelength λ, the peak-to-valley wave height W and the base diameter D, which is equal to the diameter of valley. Then the diameter of peak is $(2W+D)$. In present inertial Cartesian coordinate system, the x-, y- and z-axis are defined as streamwise, vertical and spanwise directions, respectively, as shown in Fig. 2(a). The non-dimensional control parameter for present flows is the Reynolds number, defined by $Re=U_\infty D/v$, where U_∞ is the free-stream velocity.

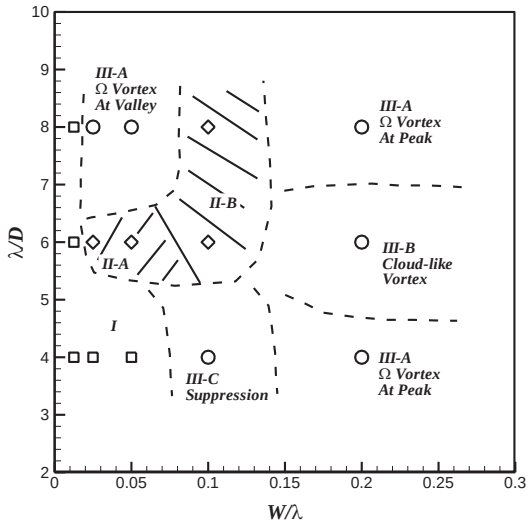

(a)

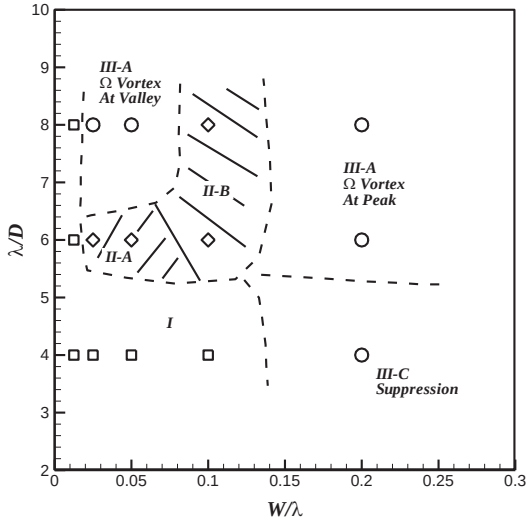

(b)

Fig. 1 Summary of the vortex patterns of (a) the harmonic and (b) conic cylinders varied with the wavelength λ/D versus the wavy steepness W/λ for all computational cases at the Reynolds number of 100, where symbols □, ◇ and ○ denote regimes I (weak disturbance), II (moderate disturbance) and III (strong disturbance), respectively. The dashed lines are boundary lines to separate different regimes. The dashed region with oblique lines denotes approximately the occurrence of regime II.

The non-dimensional forms of the continuity and Navier-Stokes equations are then written down as follows,

$$\nabla \bullet \boldsymbol{u} = 0 \tag{1a}$$

$$\frac{\partial \boldsymbol{u}}{\partial t} + (\boldsymbol{u} \bullet \nabla)\boldsymbol{u} = -\nabla p + \frac{1}{Re}\nabla^2 \boldsymbol{u} \tag{1b}$$

where t is the non-dimensional time, $\boldsymbol{u}$ the velocity vector (u,v,w), p the static pressure, and ∇ the gradient operator. In the periodic flow, the frequency of vortex shedding f is non-dimensionalized as the Strouhal number defined as $St=fD/U_\infty$. Lengths and velocities are scaled by the cylinder base diameter D and the free-stream velocity U_∞ respectively.

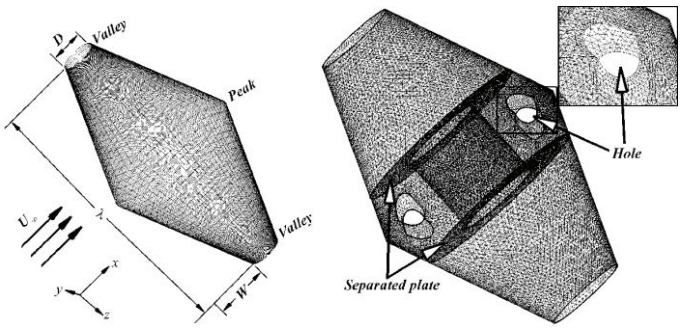

(a) (b)

Fig. 2 Schematics of flows past the circular cylinders with (a) the conic disturbance and (b) the perforated conic shroud along the span.

Numerical Method

At Re=100, direct numerical simulation (DNS) is carried out due to the laminar flow. While large eddy simulation (LES) with Smagorinsky-Lilly subgrid-scale (SGS) model is adopted in simulating turbulent wake transition at the Reynolds number of 10^5.

In simulated flow, the proper boundary conditions are proposed as follows. To simulate the infinite length of cylinder, the periodic flow along the span is assumed. Then as for boundary conditions in (x,y) plane, the uniform free-stream velocity at inlet, simple non-reflecting outflow at outlet, free slip at vertical sides and non-slip boundary condition on cylinder surface are prescribed.

Two different grid forms are adopted. As for the conic disturbance without the perforation, the structural grids are in a hexagonal form. While as for the perforated conic shroud, the non-structural grids near the shroud are in a tetrahedral form and structural grids away from the shroud are in a hexagonal form.

The non-dimensional size of computational domain for disturbed cylinder is $40\times20\times\lambda/D$ ($x\times y\times z$), as well as for the straight cylinder. A non-dimensional time step of 0.01 or 0.005 is used with the second-order time discretization. The maximal magnitude of convergence error is less than 10^{-3} for the continuity equation.

Simulations are performed by FLUENT software. The SIMPLEC algorithm is selected for the pressure-velocity coupling. The second-order discretization is applied for the pressure and the bounded central differencing scheme for the momentum. The flexible or W-cycle multiple-grid method is adopted in solving pressure. More information can be referenced in previous papers (Lin, et al., 2013; 2014b).

RESULTS AND ANALYSIS

For the conic disturbance, two independent length parameters, the non-dimensional wavelength λ/D and the wave steepness W/λ, are introduced for geometric similarity. A series of W/λ (0.0125, 0.025, 0.05, 0.1 and 0.2) and λ/D (4, 6 and 8) are taken into consideration with the constant diameter D. Therefore, the straight cylinder can be obtained by reducing W/λ down to zero and only varied with λ/D.

Moreover as for the perforated conic shroud, the diameter of holes d is introduced. Their number No and position Ag (the attack angle of incoming flow to the hole on the front stagnation point of cylinder) also have influence on the flow. As for an elementary study here, only one group of parameters (d/D=0.1, No=4, Ag=0°) is selected to investigate the effect of perforation on hydrodynamic parameters and flow patterns.

Verifications

As for the first verification of numerical simulations, three-dimensional flow past the straight circular cylinder at Re=10^5 is carried out firstly. As shown in Table 1, the Strouhal number St, the mean drag coefficient C_{D_M} and the RMS lift coefficient C_{L_RMS} obtained in present simulations are well agreed with those in previous experiments (reported in Sarpkaya and Isaacson, 1981). It should be emphasized that the force coefficient of the conic cylinder must be normalized by the free-stream dynamic pressure and the projected area of the straight cylinder with the same spanwise wavelength of the conic cylinder, rather than the projected area of the conic cylinder itself.

Table 1. Comparisons of St, C_{D_M} and C_{L_RMS} between the present simulations at Re=10^5 and experimental results in previous report.

		Present	Previous
St	λ/D=4	0.186	0.18~0.2
	λ/D=6	0.188	
	λ/D=8	0.184	
C_{D_M}	λ/D=4	1.028	1.16
	λ/D=6	1.039	
	λ/D=8	1.083	
C_{L_RMS}	λ/D=4	0.488	0.4~0.65
	λ/D=6	0.449	
	λ/D=8	0.535	

In the second verification, as shown in Fig. 2(b), separated plates are applied with a distance of 0.5D away from the peak for the sake of very weak flow with small velocity between the shroud and cylinder and then saving grid numbers and computational times. Therefore, it is also necessary to compare these hydrodynamic parameters of the perforated conic shroud with and without separated plates. As shown in Table 2, as an example, the selected case with λ/D =8 and W/λ=0.1 shows that the existence of separated plates has almost little effect.

Table 2. Comparisons of St, C_{D_M} and C_{L_RMS} with and without separated plates at the case with λ/D =8 and W/λ=0.1.

Have separated plates?	St	C_{D_M}	C_{L_RMS}
Yes	2.157	0.108	0.075
No	2.151	0.105	0.075

The conic cylinder at Re=10^5

Results of variations of the mean drag coefficient C_{D_M} and the RMS lift coefficient C_{L_RMS} along the wave steepness W/λ and non-dimensional wavelength λ/D for the flow past the conic cylinder at Re=10^5 are summarized in Fig. 3. By comparing these results with those at lower Reynolds numbers (Lin, et al., 2014b), variations of these force coefficients are similar in qualitative. The drag is increased generally as the wave steepness increases and greater than that of the straight cylinder, while the lift in cases of λ/D=6 and 8 is quickly decreased at first and then increased slowly. At λ/D=4, the lift is gradually increased and greater than that of the straight cylinder. Especially at λ/D=6, there is the local minimum of drag at W/λ=0.05. Such feature can give us a suggestion that there exists the optimized

region for specific λ/D and W/λ in structural design by applying the conic disturbance. In such region, the drag could be reduced or only increased a little with the great reduction of lift.

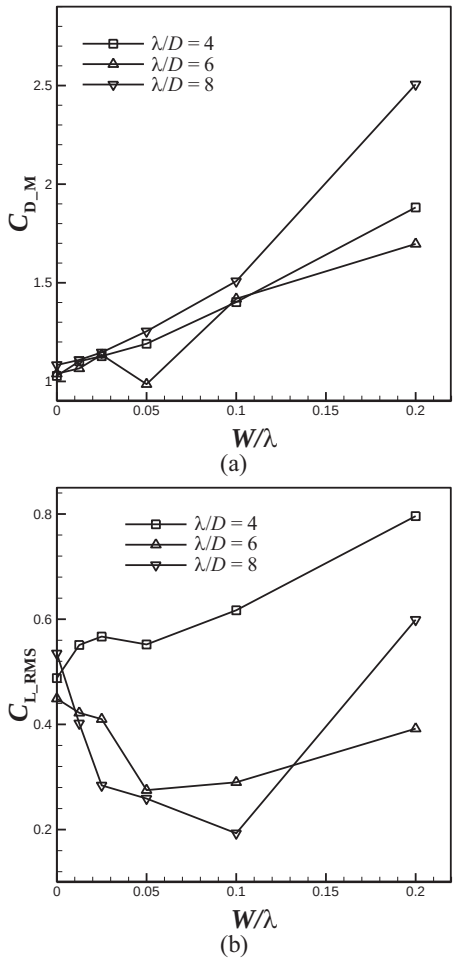

Fig. 3 Variations of the mean drag coefficient C_{D_M} and the RMS lift coefficient C_{L_RMS} along the wave steepness W/λ and non-dimensional wavelength λ/D for the flow past the conic cylinder at Re=10^5.

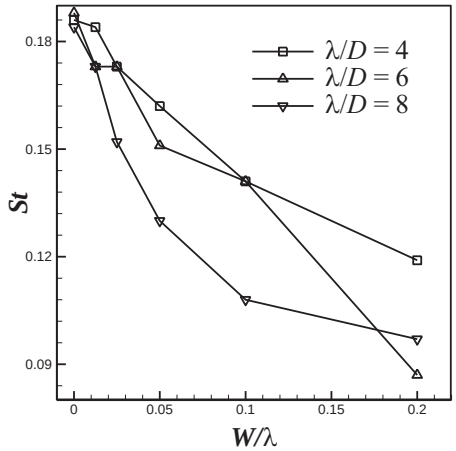

Fig. 4 Variations of the Strouhal number St with respect to W/λ and λ/D for the flow past the conic cylinder at Re=10^5.

Figure 4 presents the variation of non-dimensional frequency of vortex shedding, the Strouhal number St, obtained from the time history of total lift, with respect to W/λ and λ/D at Re=10^5. With the increasing wave steepness, St is generally decreased. This is also similar to that at lower Reynolds numbers (Lin, et al., 2014b). Such feature indicates that VIV of structure would be occurred at higher stream velocity, agreed well with the previous experiments (Lin, et al., 2012).

The perforated conic shroud at Re=10^2

Hydrodynamic parameters. After introducing the perforation on the peak of the conic cylinder, as shown in Fig. 5, drag and lift in most cases are almost a little higher or less than those without perforation. At some certain cases, such as W/λ=0.1 and λ/D=4, the drag reduction reaches 22% and the lift is greatly reduced down to zero. At a certain case with W/λ=0.2 and λ/D=8, the drag and lift are increased obviously. These different behaviors in fluid forces denote that the vortex pattern in near wake is significantly disturbed and different from the original vortex pattern in the wake of the conic cylinder without the perforation.

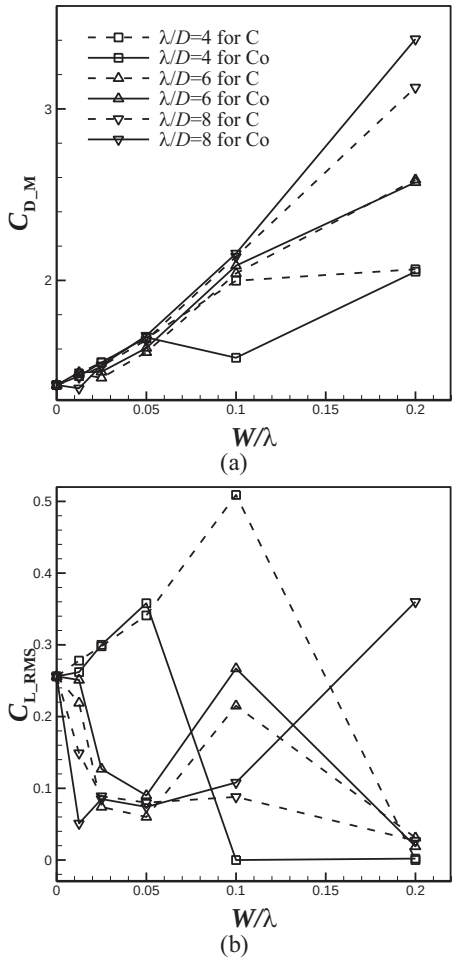

Fig. 5 Variations of the mean drag coefficient C_{D_M} and the RMS lift coefficient C_{L_RMS} along W/λ and λ/D for the flow past the perforated conic shroud (marked by "Co") at Re=10^2, and in comparison with those for the flow past the conic cylinder (marked by "C").

Correspondingly, the variation of the Strouhal number, as shown in Fig. 6, is almost invariable in most cases, but obviously different in some special cases. For example, in the case of W/λ=0.1 and λ/D=4, St=0, while it is increased greatly in the case of W/λ=0.2 and λ/D=8.

Vortex patterns in the near wake. As shown in Fig. 7, different

disturbance regimes are identified based on effects of the introduced perforation on the vortex patterns in the near wake. By comparing with that for the conic cylinder without the perforation in Fig. 1(b), it shows that the regime II of moderate disturbance is extended to neighbor regimes I and III for weak and strong disturbances, while the regime III of strong disturbance only extends to the original regime I of weak disturbance at small W/λ and λ/D for the conic cylinder.

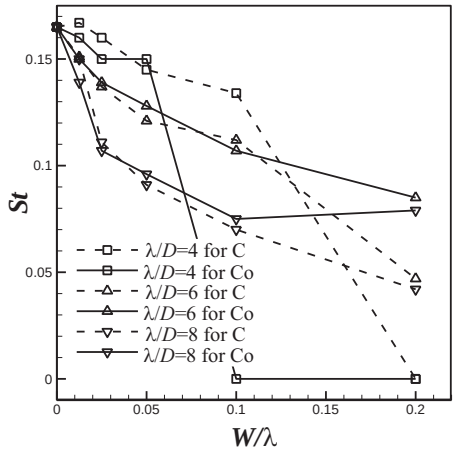

Fig. 6 Variations of the Strouhal number St with respect to W/λ and λ/D for the flow past the perforated conic shroud (marked by "Co") at $Re=10^2$, and in comparison with that for the flow past the conic cylinder (marked by "C").

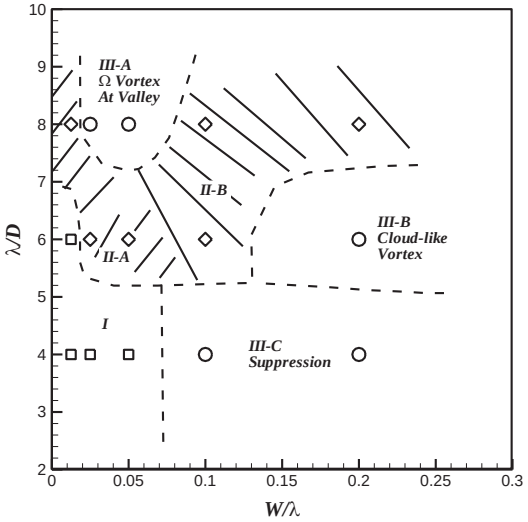

Fig. 7 Summary of the vortex patterns of the perforated conic shroud varied with the wavelength λ/D versus the wavy steepness W/λ for all computational cases at $Re=100$, where symbols □, ◇ and ○ denote regimes I (weak disturbance), II (moderate disturbance) and III (strong disturbance), respectively. The dashed lines are boundary lines to separate different regimes. The dashed region with oblique lines denotes approximately the occurrence of regime II.

These different vortex patterns caused by the perforation are presented as follows. As for the original weak disturbance for the conic cylinder in the case of $W/\lambda=0.0125$ and $\lambda/D=8$, spanwise vortex pairs are still shed alternatively but distorted mainly by the streamwise vortex pairs, as shown in Fig. 8. The vertical vortex pairs die away downstream. This feature is classified as the regime II-A of moderate disturbance.

In the case of $W/\lambda=0.2$ and $\lambda/D=8$, the perforation weakens the strong effect of conic disturbance in the regime III-A with the Ω-type vortex shed at the peak into the moderate disturbance in the regime II-B with spanwise vortex pairs distorted by the streamwise and vertical vortex pairs, as shown in Fig. 9.

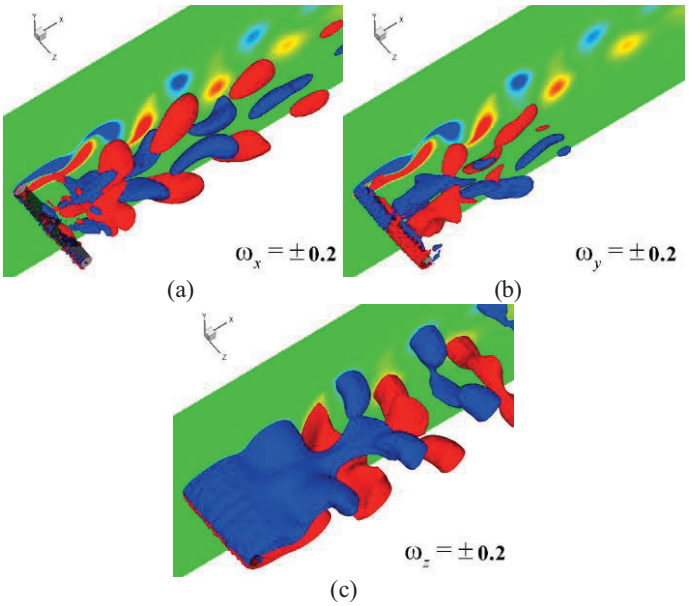

Fig. 8 Perspective views for iso-surfaces of (a) ω_x, (b) ω_y and (c) ω_z in the case of the perforated conic cylinder with $\lambda/D=8$ and $W/\lambda=0.0125$. The positive value is red and the negative value blue. The slice at the end of cylinder is the contour of ω_z varied from -0.5 to 0.5. The body is shown by the translucent cylinder with a black frame (same below).

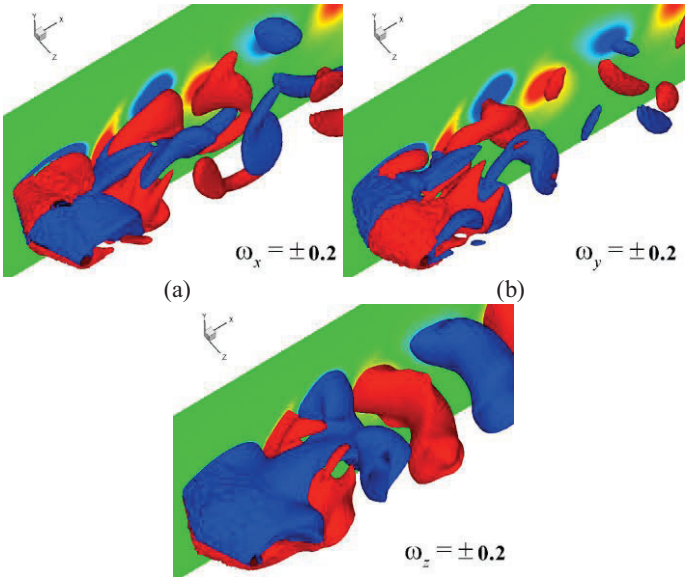

Fig. 9 Perspective views for iso-surfaces of (a) ω_x, (b) ω_y and (c) ω_z in the case of the perforated conic cylinder with $\lambda/D=8$ and $W/\lambda=0.2$.

As shown in Fig. 10 for the case of $W/\lambda=0.2$ and $\lambda/D=6$, the effect of introducing perforation is still in the strong disturbance. But the vortex pattern is varied from the Ω-type vortex shed at the peak to the cloud-like vortex, which is like that in the near wake of the cylinder with harmonic disturbance, as shown in Fig. 1(a). Furthermore, iso-surfaces of spanwise vorticity have shown that the cloud-like vortex actually

consists of two groups of the Ω-type vortex alternatively shed at the peak and valley respectively.

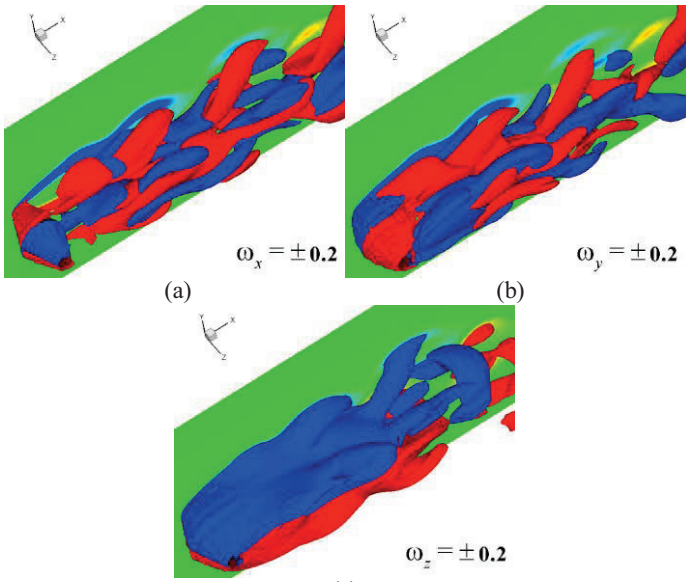

(a) (b) (c)

Fig. 10 Perspective views for iso-surfaces of (a) ω_x, (b) ω_y and (c) ω_z in the case of the perforated conic cylinder with λ/D=6 and W/λ=0.2.

Interestingly in the case of W/λ=0.1 and λ/D=4, as shown in Fig. 11, the original weak disturbance becomes the strong disturbance coupled with the effect of perforation. The vortex shedding alternatively is totally suppressed. The streamwise vorticity is obviously weaker than the vertical vorticity and disappeared downstream. The upper and lower shear layers behind the body become steady and extend far away downstream. It is confirmed again that the physical mechanism for the complete suppression of Kármán vortex shedding is mainly attributed to the vertical vorticity, rather than the streamwise vorticity.

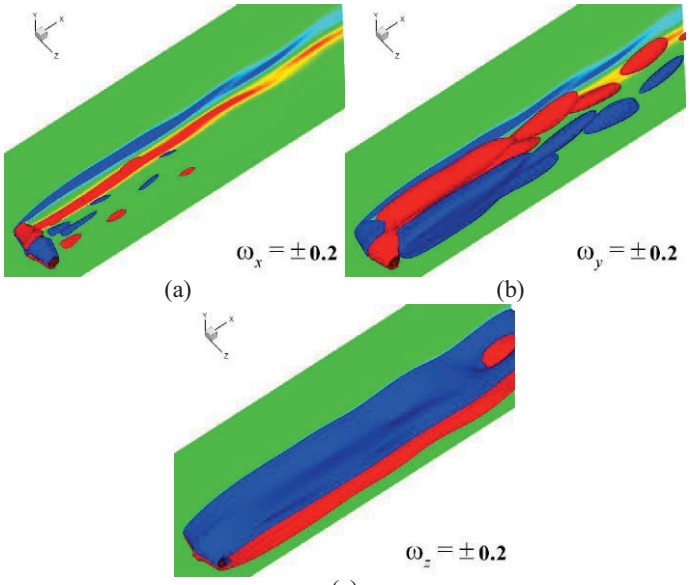

(a) (b) (c)

Fig. 11 Perspective views for iso-surfaces of (a) ω_x, (b) ω_y and (c) ω_z in the case of the perforated conic cylinder with λ/D=4 and W/λ=0.1.

CONCLUSIONS

In present paper, flows past the circular cylinder with the conic disturbance at the higher Reynolds number of 10^5 and coupled with the introduction of perforation on the conic shroud at the lower Reynolds number of 10^2 are numerically simulated with a series of different wavelength and wave steepness.

Through the comparison with results of the conic cylinder at lower Reynolds numbers, variations of hydrodynamic parameters, such as the drag and lift coefficients and the Strouhal number, in most cases are qualitatively similar along with the increasing wave steepness. This indicates that features of hydrodynamic parameters are little influenced by the Reynolds number varied in the range of 10^2 to 10^5.

When the perforation on the peak of conic disturbance is introduced, qualitative variations of hydrodynamic parameters are still similar to those of the conic cylinder. However, from the point of the extent of disturbance on the flow, there are several changes on the board of different disturbance regimes. Noticeably, the moderate disturbance in the regime II extends to the neighbor regimes.

Correspondingly, different vortex patterns in the near wake of the perforated conic shroud are identified. This demonstrates that the introduction of perforation leads to significant evolutions in the vortex shedding, such as the complete suppression of vortex shedding in the case of λ/D=6 and W/λ=0.2, and the cloud-like vortex originated from the Ω-type vortex shed at the peak in the case of λ/D=8 and W/λ=0.2.

In future works, a series of different parameters, the number of holes, their size and attack angle, are selected to investigate their effects on the hydrodynamic parameters and flow patterns. As a basic reference, this could be used for the preliminary design in the later experiment.

ACKNOWLEDGEMENTS

The authors sincerely acknowledge the support of the National Key Scientific Instrument and Equipment Development Program of China (No. 2011YQ120048) for the work reported in this paper.

REFERENCES

Assi, GRS, Bearman, PW, and Kitney, N (2009). "Low drag solutions for suppressing vortex-induced vibration of circular cylinders," *J Fluids Struct*, 25, 666–675.

Bearman, PW, and Owen, JC (1998). "Reduction of bluff-body drag and suppression of vortex shedding by the introduction of wavy separation lines," *J Fluids Struct*, 12, 123–130.

Gabbai, RD, and Benaroya, H (2005). "An overview of modeling and experiments of vortex-induced vibration of circular cylinders," *J Sound Vib*, 282, 575-616.

Huang, S (2011). "VIV suppression of a two-degree-of-freedom circular cylinder and drag reduction of a fixed circular cylinder by the use of helical grooves," *J Fluids Struct*, 27, 1124–1133.

King R, Brown A, and Braaten H, et al. (2013). "Suppressing full-scale riser VIV with the VT suppressor," *Proc 32nd Int. Conf. on Ocean, Offshore and Arctic Eng.* OMAE, Nantes, France, OMAE2013-11642.

Korkischko, I, and Meneghini, JR (2010). "Experimental investigation of flow-induced vibration on isolated and tandem circular cylinders fitted with strakes," *J Fluids Struct*, 26, 611-625.

Korkischko, I, and Meneghini, JR (2012). "Suppression of vortex-induced vibration using moving surface boundary-layer control," *J Fluids Struct*, 34, 259–270.

Kumar, RA, Sohn, CH, and Gowda, BHL (2008). "Passive control of

vortex-induced vibrations: an overview," *Recent Patents on Mechanical Eng*, 1(1), 1-11.
Lee, L, and Allen, DW (2005). "The dynamic stability of short fairings," *Offshore Tech Conf*, Houston, Texas, USA, OTC-17125.
Lin, LM, Ling, GC, and Wu, YX (2010). "Mechanism responsible for the complete suppression of Karman vortex in flows past a wavy square-section cylinder," *Chin Phy Let*, 27, 034702.
Lin, LM, Zhong, XF, and Wu, YX (2011). "Experimental investigation of a new device in suppressing vortex-induced vibrations of a circular cylinder," *Proc 21st Int Offshore and Polar Eng Conf*, Maui, Hawaii, ISOPE, 3, 1283–1288.
Lin, LM, Zhong, XF, and Wu, YX (2012). "Vortex-induced vibrations of a circular cylinder with different geometric disturbances," *Proc 22nd Int Offshore and Polar Eng Conf*, Rhodes, Greece, ISOPE, 3, 623–629.
Lin, LM, Zhong, XF, and Wu, YX (2013). "Flow around a circular cylinder with radial disturbances at a low Reynoldsnumber," *Proc 23rd Int Offshore and Polar Eng Conf*, Anchorage, Alaska, USA, ISOPE, 3, 387–394.
Lin, LM, Zhong, XF, and Wu, YX (2014a). "Characteristics for a flow past a circular cylinder with two types of radial disturbances at Re=100," *Advanced Materials Research*, 871, 107–114.
Lin, LM, Zhong, XF, and Wu, YX (2014b). "The drag, Lift and Strouhal number of a circular-section cylinder with a conic disturbance at subcritical Reynolds numbers," *Proc33rd Int Conf Ocean, Offshore and Arctic Eng*, OMAE2014, San Francisco, California, USA, OMAE2014-23017.
Owen, JC, Bearman, PW, and Szewczyk, AA (2001). "Passive control of VIV with drag reduction," *J Fluids Struct*, 15, 597-605.
Owen, JC, Szewczyk, AA, and Bearman, PW (1999). "Suppressing Kármán vortex shedding by use of sinuous circular cylinders," *Bulletin of the American Physical Society*, 44, 124.
Sarpkaya, T (1979). "Vortex-Induced Oscillations — A Selective Review," *J Appl Mech*, 46, 241-258.
Sarpkaya, T (2004). "A critical review of the intrinsic nature of vortex-induced vibrations," *J Fluids Struct*, 19, 389-447.
Sarpkaya, T, and Isaacson, M (1981). *Mechanics of wave forces on offshore structures*. Van Nostrand Reinhold Company, New York, USA, 606.
Trim, AD, Braaten, H, Lie, H, and Tognarelli, MA (2005). "Experimental investigation of vortex-induced vibration of long marine risers," *J Fluid Struct*, 21, 335-361.
Williamson, CHK, and Govardhan, R (2004). "Vortex-induced vibrations," *Annu Rev Fluid Mech*, 36, 413-455.
Williamson, C.H.K. and Govardhan, R (2008). "A brief review of recent results in vortex-induced vibrations," *J Wind Eng Ind Aerodyn*, 96, 713-735.
Wu, H, and Sun, DP (2009). "Study on suppression measures for vortex-induced vibration of the deepwater riser," *China Offshore Platform*, 24, 1-8.
Wu, H, Sun, DP. and Lu, L. et al. (2012). "Experimental investigation on the suppression of vortex-induced vibration of long flexible riser by multiple control rods," *J Fluids Struct*, 30, 115–132.